Research Square

Preprints are preliminary reports that have not undergone peer review.
They should not be considered conclusive, used to inform clinical practice,
or referenced by the media as validated information.

# Environmental PFOSA Exposure Activates NF-κB and Disrupts Lysosomal Gb3 Metabolism in Renal Tubular Cells

**Yu Zhang**
Yunnan Center for Disease Control and Prevention (Yunnan Academy of Preventive Medicine)
**Xue Yang**
Yunnan Center for Disease Control and Prevention (Yunnan Academy of Preventive Medicine)
**Minghao Zhai**
Yunnan Center for Disease Control and Prevention (Yunnan Academy of Preventive Medicine)
**Qingjian Zhao**
Yunnan Center for Disease Control and Prevention (Yunnan Academy of Preventive Medicine)
**Liming Jiang**
Ningbo University
**Ni Ma**
Yunnan Center for Disease Control and Prevention (Yunnan Academy of Preventive Medicine)
**Zushun Yang**
Yunnan Center for Disease Control and Prevention (Yunnan Academy of Preventive Medicine)
**Min Liu**
Yunnan Center for Disease Control and Prevention (Yunnan Academy of Preventive Medicine)
**Min Chen**
chenmin@yncdc.cn

Yunnan Center for Disease Control and Prevention (Yunnan Academy of Preventive Medicine)

**Research Article**

**Keywords:** PFOSA, AKI, Early apoptosis, NF-κB signaling pathway, Gb3 accumulation, Environmental toxicology

**Posted Date:** November 24th, 2026

**DOI:** https://doi.org/10.21203/rs.3.rs-11328158/v1

**License:** This work is licensed under a Creative Commons Attribution 4.0 International License.
Read Full License

**Additional Declarations:** No competing interests reported.

# Environmental PFOSA Exposure Activates NF-κB and Disrupts Lysosomal Gb3 Metabolism in Renal Tubular Cells

Yu Zhang[1,2,3#], Xue Yang[3#], Minghao Zhai[3], Qingjian Zhao[3], Liming Jiang[4], Ni Ma[3], Zushun Yang[1,2,3], Min Liu[1,2,3], Min Chen[1,2,3*]

1. Yunnan International Joint Laboratory of Public Health and Disease Control, Yunnan Center for Disease Control and Prevention (Yunnan Academy of Preventive Medicine), Kunming, Yunnan, China

2. Yunnan Provincial Key Laboratory of Public Health and Biosafety, Yunnan Center for Disease Control and Prevention (Yunnan Academy of Preventive Medicine), Kunming, Yunnan, China

3. Health Laboratories Center, Yunnan Center for Disease Control and Prevention (Yunnan Academy of Preventive Medicine), Kunming, Yunnan, China

4. School of Basic Medical Sciences, Health Science Center, Ningbo University, Ningbo, Zhejiang, China

**Abstract:** Ammonium perfluorooctane sulfonate (PFOSA), a widely distributed surfactant salt of perfluorooctane sulfonic acid (PFOS), bioaccumulates in aquatic systems and biota, exerting multi-system toxicity. Although hepatotoxicity, immunotoxicity, and neurotoxicity are well characterised, the molecular mechanisms underlying PFOSA-induced renal injury remain poorly defined. This study aimed to elucidate the intracellular mechanisms linking environmentally relevant PFOSA exposure to renal tubular cell death. Human renal proximal tubular epithelial (HK2) cells were exposed to PFOSA (0.5–5 μM). Cell viability, apoptosis, acute kidney injury (AKI) biomarkers, and transcriptomic changes were assessed using CCK-8, flow cytometry, TUNEL staining, RT-qPCR, RNA sequencing, and ELISA. PFOSA induced concentration- and time-dependent cytotoxicity ($IC_{50}$ = 4.937 μM), doubled the early apoptotic fraction, and elevated AKI biomarkers including kidney injury molecule-1 (KIM-1) and N-acetylglucosaminidase (NAGLU). RNA sequencing revealed dual mechanisms: (i) NF-κB p50/p52 upregulation coupled with transcriptional suppression of anti-apoptotic BIRC2/5 and down-regulation of FAS/HRK, shifting the balance toward TP53-driven apoptosis; and (ii) a putative RPL36A–HNRNPH2 read-through fusion associated with GLA silencing, resulting in lysosomal globotriaosylceramide (Gb3) accumulation and apoptotic amplification. These findings establish NF-κB reprogramming and GLA–Gb3

# Coauthors- Yu Zhang and Xue Yang contributed equally.

* Corresponding author.
Email addresses: chenmin@yncdc.cn(Min Chen).

lysosomal dysregulation as novel molecular nodes of PFOSA nephrotoxicity at environmentally relevant concentrations, offering potential dual-target therapeutic strategies against PFAS-induced renal injury.

**Keywords:** PFOSA; AKI; Early apoptosis; NF-κB signaling pathway; Gb3 accumulation; Environmental toxicology

## 1. Introduction

Ammonium perfluorooctane sulfonate (PFOSA), a major salt-type derivative of perfluorooctane sulfonate, is widely used in fire-fighting foams, electroplating baths, textile finishes, and semiconductor production. The C–F backbone of PFOSA—among the strongest single bonds in organic chemistry—confers exceptional resistance to acids, bases, and thermal degradation. Consequently, natural attenuation is negligible, and PFOSA has become a ubiquitous environmental contaminant. Concentrations in soils reach 0.1–1 μg/g; ground and surface waters routinely contain 0.5–200 ng/L, with hotspots exceeding 1 μg/L. Long-range atmospheric transport facilitates global distribution, and bioaccumulation has been documented across diverse taxa including fish, birds, and mammals[1].

The molecular structure of PFOSA, the ammonium salt of perfluorooctane sulfonic acid (PFOS), is shown in Fig. 1A. It comprises a perfluorooctyl chain ($C_8F_{17}$–) covalently linked to a sulfonate group (–$SO_3^-$), electrostatically paired with an ammonium ion ($NH_4^+$). The C–F bonds of the perfluoroalkyl backbone (bond dissociation energy ~540 kJ/mol) confer marked chemical and thermodynamic stability, whereas the terminal ionic pair ensures high aqueous solubility and pronounced surface activity[2]. These physicochemical properties—persistence, solubility, and surface activity—collectively drive environmental dispersion, bioavailability, and cellular uptake, predisposing biota to toxic effects.

Epidemiological and experimental studies consistently associate PFOSA exposure with adverse health outcomes. The compound is absorbed via drinking water, food, and inhalation, binds avidly to plasma proteins, and persists in the body with a half-life of three to five years[3]. Hepatotoxicity is among the most characterized effects: PFOSA induces hepatomegaly, steatosis, and oxidative stress through PPARα/γ activation coupled with inhibition of mitochondrial β-oxidation, resulting in elevated liver enzymes and perturbed lipid metabolism[4]. Immunotoxicity manifests as Th1 suppression and impaired antibody affinity maturation, compromising responses to vaccines and pathogens[5]. Thyroid disruption follows from inhibition of thyroid peroxidase and blockage of thyroglobulin iodination, producing decreased circulating T3 and T4 with compensatory TSH elevation. Reproductive and developmental toxicity includes reduced testosterone synthesis and sperm motility in males, impaired follicular maturation and estrous cycle disruption in females, and low birth weight with neurobehavioural deficits in offspring[6]. Neurotoxicity arises from blood–brain barrier penetration, hippocampal neuronal apoptosis, and gliosis, resulting in measurable deficits in learning and memory [7]; Cardiotoxicity, even at chronic low doses, involves mitochondrial membrane potential collapse and calcium dyshomeostasis in cardiomyocytes, increasing arrhythmia

susceptibility[8-10]. Renal toxicity remains comparatively understudied, despite the kidney being a primary route of PFOSA elimination and a known target of PFOS-related pathology. Collectively, these data indicate that PFOSA exerts multi-system toxicity affecting the liver, kidneys, immune system, thyroid, reproductive system, nervous system, and cardiovascular system. Given that PFOS is listed as a persistent organic pollutant under the Stockholm Convention, characterizing the environmental fate and toxicological profile of its ammonium salt is critical for risk assessment and regulatory decision-making.

The intracellular mechanisms linking PFOSA exposure to renal cell death, however, remain poorly resolved. To address this gap, we exposed human HK2 (proximal tubular epithelial) and 293T (embryonic kidney) cells to PFOSA and examined the resultant molecular alterations. Acute exposure activated the NF-κB pathway and amplified pro-apoptotic signaling, while concomitantly suppressing GLA expression. The ensuing reduction in α-galactosidase A activity led to lysosomal accumulation of globotriaosylceramide (Gb3), which triggered renal cell apoptosis. These findings establish a direct mechanistic link between PFOSA exposure and programmed cell death, and identify lysosomal Gb3 accumulation as a novel mediator of PFOSA-induced nephrotoxicity.

## 2. Materials and methods

### 2.1. Cell culture and compound exposure

HK2 and 293T cells were purchased from Procell Life Science & Technology (Wuhan, China). HK2 cells were maintained in Minimum Essential Medium (MEM; VivaCell) supplemented with 10% fetal bovine serum (FBS; VivaCell), 100 U/mL penicillin, and 100 μg/mL streptomycin (Sigma-Aldrich). 293T cells were cultured in Dulbecco's Modified Eagle Medium (DMEM; VivaCell) containing the same antibiotic cocktail and 10% FBS. All cultures were incubated at 37 °C in a humidified atmosphere of 5% $CO_2$ as two-dimensional monolayers and routinely screened for mycoplasma contamination using the MycoSEQ™ Plus Mycoplasma Detection Kit (Thermo Fisher Scientific). Cell stocks were discarded once the cumulative passage number exceeded 30.

The test compound, ammonium perfluorooctane sulfonate (PFOSA), was supplied as a 1M stock solution in methanol. Vehicle controls receiving an equivalent volume of methanol were included in every experiment. Cells were subjected to varying exposure durations and PFOSA concentrations. After exposure, cell viability, apoptosis, and the expression of acute kidney injury-related genes were assessed.

### 2.2. Cell viability assay(CCK-8)

Adherent HK2 cells were detached with 0.25% trypsin–EDTA, washed once with ice-cold PBS, and resuspended in the same buffer. After trypan blue exclusion staining, viable cells were enumerated with a hemocytometer and randomly allocated into treatment and vehicle groups (n = 6 replicates per group). A total of 2 × $10^3$ cells in 100 μL complete MEM were seeded into each well of a 96-well plate and allowed to attach for 12 h. The medium was then replaced with fresh complete MEM containing serial dilutions of PFOSA, and cells were

cultured for the designated periods. At each time point, 10 μL CCK-8 reagent was added to each well, followed by 1 h incubation under standard culture conditions. Absorbance at 450 nm ($A_{450}$) was measured with a microplate reader; higher $A_{450}$ values indicate greater cell viability.

### 2.3. Real-time quantitative PCR (RT-qPCR)

Total RNA was isolated using the Eastep® Super Total RNA Extraction Kit (Promega, Shanghai, China), and its concentration and purity ($A_{260}/A_{280} \geq 1.95$) were verified on a Thermo Scientific™ NanoDrop™ One micro-volume spectrophotometer. First-strand cDNA was synthesized from 1 μg RNA using Eastep RT Master Mix (5×). Quantitative real-time PCR was performed with Hieff UNICON® Universal Blue qPCR SYBR Green Master Mix (Yeasen, Shanghai, China) on a ViiA™ 7 Real-Time PCR system (Applied Biosystems, Foster City, CA, USA). β-Actin served as the endogenous reference, and relative gene expression was calculated by the $2^{-}$^ΔΔCt method. Primer sequences are listed in Supplementary Table 1.

### 2.4. Flow-cytometric apoptosis assay

For apoptosis detection, cells were stained with the Annexin V-FITC Apoptosis Detection Kit (Beyotime, Shanghai, China). Adherent cells were detached with 0.25% trypsin–EDTA, washed twice with ice-cold PBS, and resuspended in 1× Binding Buffer. Cells were then sequentially incubated with 5 μL Annexin V-FITC and 5 μL propidium iodide (PI, 50 μg/mL) for 15 min in the dark. Immediately before acquisition, 400 μL Binding Buffer was added. Samples were analyzed on a BD FACSCanto™ II flow cytometer (BD Biosciences) using 488 nm excitation; FITC (FL1) and PI (FL2) emissions were collected for a minimum of $1 \times 10^4$ events per sample. Compensation and quadrant analyses were performed with FlowJo v10.8. Cells positive for Annexin V-FITC and negative for PI (Annexin $V^+/PI^-$) were defined as early apoptotic; early apoptosis rate (%) = (Annexin $V^+/PI^-$ cells) / (total cells) × 100%.

### 2.5. TUNEL assay

In six-well plates, HK2 and 293T cells were seeded separately on tissue-culture-treated coverslips and exposed to PFOSA in complete medium for 72 h. After medium removal, cells were rinsed twice with PBS and fixed with 4% paraformaldehyde for 30 min at room temperature, followed by three PBS washes. Cells were permeabilized with 0.2% Triton X-100 for 10 min at room temperature and washed again with PBS. The One-step TUNEL Apoptosis Detection Kit (GLPBIO, USA) was used according to the manufacturer's instructions: 50 μL of 1× Equilibration Buffer was applied to each sample and incubated for 10 min at room temperature; excess buffer was removed with absorbent paper. Subsequently, 50 μL of TUNEL reaction mixture (fluorescein-dUTP plus terminal deoxynucleotidyl transferase) was added to each sample and incubated for 60 min at 37 °C in the dark. After PBS rinses, nuclei were counterstained with 10 μg/mL DAPI for 5 min, and coverslips were mounted with

antifade reagent. Images were acquired under a fluorescence microscope at excitation/emission wavelengths of 550/570 nm (TUNEL) and 356/451 nm (DAPI). Five random high-power fields (×400) per coverslip were captured; TUNEL-positive and total cells were counted with ImageJ, and the apoptotic rate was expressed as the percentage of TUNEL-positive cells. All experiments were performed in triplicate.

### 2.6. Enzyme-linked immunosorbent assay(ELISA)

For intracellular component analysis, adherent HK2 and 293T cells were detached with trypsin, washed twice with ice-cold PBS, and resuspended in ice-cold PBS at $1 \times 10^6$cells/mL. Complete cell disruption and release of intracellular contents were achieved by three freeze–thaw cycles. The lysate was centrifuged at 3,000 × g for 20 min at 4 °C, and the supernatant was carefully collected. Concentrations of GLA protein and globotriaosylceramide (Gb3) were determined with the Human GLA ELISA Kit and Human Gb3 ELISA Kit (COIBOBIO, Shanghai, China), respectively, following the manufacturer's instructions.

### 2.7. Western blot

Cells were lysed in RIPA buffer (Beyotime, China), and protein concentrations were determined by the BCA method. A total of 30 μg protein per sample was separated by SDS-PAGE and transferred onto PVDF membranes (Millipore, Germany). Membranes were blocked with 2% BSA at room temperature for 1 hour, followed by overnight incubation at 4℃ with the following primary antibodies: anti-GLA (Proteintech, Cat No. 66121-1-Ig, 1:1000), anti-IκBα (Proteintech, Cat No. 10268-1-AP, 1:1000), anti-p-IκBα (Proteintech, Cat No. 82349-1-RR, 1:1000), anti-KIM-1 (Proteintech, Cat No. 30948-1-AP, 1:1000), anti-DKK3 (Proteintech, Cat No. 10365-1-AP, 1:1000), anti-TIMP2 (Proteintech, Cat No. 85882-2-RR, 1:1000), and anti-GAPDH (Proteintech, cat. no. 10494-1-AP, 1:1000). The following day, membranes were incubated with HRP-conjugated secondary antibodies at room temperature for 1 hour. Immunoreactive bands were visualized using Immobilon ECL Ultra Western HRP Substrate (Millipore) and exposed to X-ray film.

### 2.8. RNA sequencing and bioinformatics analysis

Total RNA was extracted from each group of cells using TRIzol® Reagent (Invitrogen). After DNase I digestion to remove genomic DNA, RNA integrity was verified on an Agilent 2100 Bioanalyzer (RIN ≥ 7.0). Strand-specific libraries were constructed from 2 μg RNA as follows: (i) mRNA enrichment with the NEBNext®

Poly(A) mRNA Magnetic Isolation Module; (ii) fragmentation and double-stranded cDNA synthesis; (iii) end-repair, dA-tailing, and adapter ligation; (iv) 12-cycle PCR amplification and purification. Qualified libraries were sequenced on an Illumina NovaSeq 6000 platform in PE150 mode, yielding ≥ 20 Gb clean reads per sample. Adapter sequences and low-quality reads were trimmed with fastp (v0.23). Clean reads were aligned to the GRCh38/hg38 reference genome using HISAT2 (v2.2.1), and gene-level quantification was performed with featureCounts (v2.0.3). Differential expression analysis was conducted with DESeq2 (v1.34); genes with $|\log_2 FC| \geq 1.5$ and FDR < 0.001 were considered significant. GO and KEGG enrichment analyses together with graphical outputs were generated with the online tools provided by GeneDenovo Biotechnology Co., Ltd and Be Creative Lab Co., Ltd. The RNA sequencing data reported in this study have been deposited in the Genome Sequence Archive for Human (GSA-Human: HRA018645) at the National Genomics Data Center/China National Center for Bioinformation (NGDC/CNCB), publicly accessible at https://ngdc.cncb.ac.cn/gsa-human[11,12].

### 2.9. Statistical analysis

All experiments were performed independently at least three times. Statistical analyses and graphing were conducted with SPSS 19.0 and GraphPad Prism (v8.3). Normality and homogeneity of variance were assessed for all continuous variables. Normally distributed data are presented as mean ± standard deviation (SD). Comparisons between two groups were performed using two-tailed Student's t-test, and multiple groups were compared by one-way analysis of variance (ANOVA) followed by Tukey's honestly significant difference (HSD) post-hoc test. For data that violated normality or homogeneity of variance, non-parametric tests were applied: the Mann-Whitney U test for two-group comparisons and the Kruskal-Wallis test followed by Dunn's post-hoc test for multiple-group comparisons. Statistical significance was set at $P < 0.05$.

## 3. Results

### 3.1. PFOSA exposure reduces the viability of renal proximal tubular epithelial cells

To evaluate the impact of ammonium perfluorooctane sulfonate (PFOSA) on renal cell viability, HK2 human proximal tubular epithelial cells were exposed to complete medium containing various concentrations of PFOSA for 4 days. Cell viability was subsequently measured using the CCK-8 assay. As shown in Fig. 1B, PFOSA suppressed cell viability in a concentration-dependent manner within the 0.5–2.0 μM range. Non-linear regression analysis yielded an $IC_{50}$ of 4.937 μM after 4 days of exposure, indicating pronounced low-micromolar cytotoxicity of PFOSA toward HK2 cells.

To determine the time-dependent cytotoxicity of PFOSA, HK2 cells were cultured in complete medium containing4.937 μM PFOSA for up to seven five days, with cell viability assessed daily using the CCK-8 assay. As shown in Fig. 1C, the most significant decrease in viability occurred within the first 3.605 days, suggesting rapid accumulation of toxic injury following short-term exposure. These data demonstrate that PFOSA-induced

cytotoxicity is characterized by a significant time-cumulative effect.

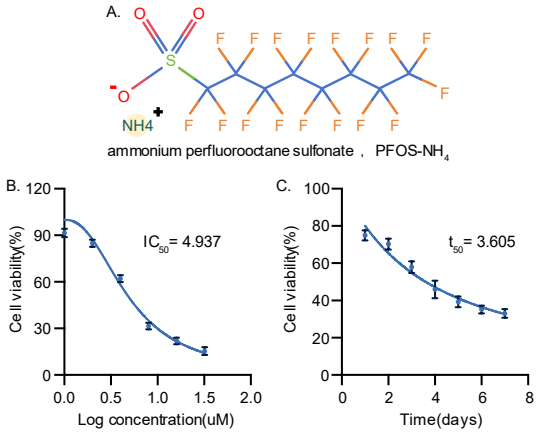



**Fig. 1.** Chemical structure and cytotoxic evaluation of ammonium perfluorooctane sulfonate. (A) Molecular structure of PFOSA: one $C_8$ perfluoroalkyl chain linked to a sulfonate head group. (B) HK2 viability after 4 d exposure to graded PFOSA concentrations; sigmoidal dose-response curve yielded an $IC_{50}$ of 4.937 µM. (C) Time-dependent viability of HK2 cells exposed to 4.937 µM PFOSA; the time required for 50% viability loss ($t_{50}$) was 3.605 days. Data are mean ± SD; n = 6.

### 3.2. PFOSA exposure upregulates AKI biomarker expression

To evaluate whether PFOSA exposure precipitates acute kidney injury (AKI), HK2 cells were challenged with 5 µM PFOSA for 3.5 days, and AKI-related transcripts were quantified by RT-qPCR. Compared with the vehicle control group, the mRNA levels of NAGLU, DKK3, IL18, OPN, TIMP2, and IGFBP7 were all significantly elevated, with the largest increases observed for KIM-1 and NAGLU (Fig. 2). These results suggest that sub-cytotoxic concentrations of PFOSA are sufficient to trigger a pronounced AKI-like transcriptional response in tubular epithelial cells and identify KIM-1 and NAGLU as sensitive, early responders to PFOSA exposure.

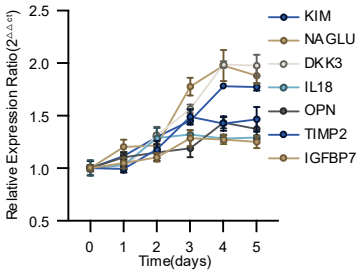



**Fig. 2.** Temporal expression profiles of AKI-related genes in HK2 cells exposed to 5 µM PFOSA for the indicated durations, assessed by RT-qPCR. Transcript levels of KIM-1, NAGLU, DKK3, IL-18, OPN, TIMP2, and IGFBP7 increased progressively with exposure time. Data are mean ± SD; *$P < 0.05$, **$P < 0.01$, ***$P < 0.001$; n = 3.

### 3.3. PFOSA exposure induces renal cell apoptosis

To corroborate the pro-apoptotic effect of PFOSA, apoptosis was quantified by flow cytometry and TUNEL staining. After 3.5-day exposure to 5 µM PFOSA, flow cytometric analysis revealed that the early-apoptotic

fraction rose from ~2% to ~8% in HK2 cells and from ~3% to ~12% in 293T cells (both $P < 0.001$ versus controls, Fig. 3A and Fig. S1), indicating robust induction of early apoptosis. Consistently, TUNEL-Cy3 fluorescence was markedly increased in both cell lines following PFOSA treatment, confirming a significant increase in apoptotic nuclei (Fig. 3B).

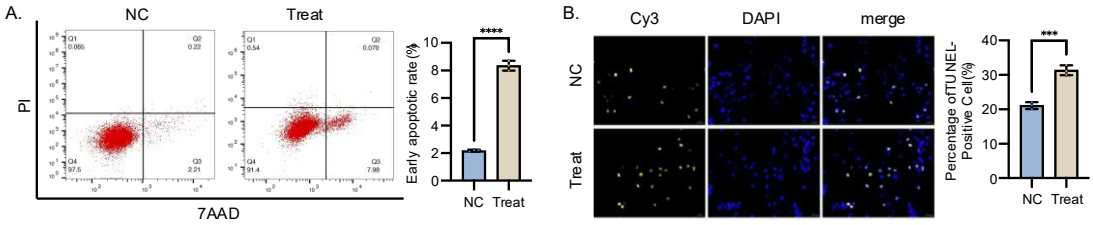



**Fig. 3.** Apoptosis assessment in HK2 cells after 3.5 d exposure to 5 μM PFOSA. (A) Flow-cytometric Annexin V-FITC/7-AAD dual staining; early apoptotic populations increased significantly. (B) TUNEL-Cy3 fluorescence; markedly elevated TUNEL-positive nuclei (yellow) indicate extensive DNA fragmentation following PFOSA exposure. Data are mean ± SD; *$P < 0.05$, **$P < 0.01$, ***$P < 0.001$; n = 3.

### 3.4. Transcriptomic profiling reveals functional consequences of PFOSA exposure in HK2 cells

To analyze the biological pathways affected by PFOSA in renal epithelia, total RNA was extracted from HK2 cells treated with 5 μM PFOSA for 3.5 days and subjected to Illumina RNA-seq. Using the criteria $|\log_2 FC| \geq 1.5$ and FDR < 0.01, 33 up-regulated and 381 down-regulated genes were identified. Gene Ontology (GO) enrichment analysis showed that the differentially expressed genes (DEGs) predominantly clustered in molecular binding events, particularly protein–nucleic acid interactions and catalytic activities (Fig. 4A), implying that PFOSA primarily disrupts networks governing nitrogen-containing macromolecule metabolism, thereby compromising essential nuclear and cytoplasmic protein functions. KEGG pathway analysis further demonstrated significant enrichment of DEGs in "cell growth and death" modules (Fig. 4B), indicating that PFOSA evokes cytotoxicity by concurrently triggering apoptosis, cell-cycle arrest, oxidative stress, and lipid metabolic perturbation. Detailed inspection of the "cell growth and death" subnetwork confirmed apoptosis as the most prominently activated pathway in PFOSA-exposed HK2 cells. Guided by these transcriptomic findings, we next interrogated the NF-κB signaling axis as a candidate mediator of PFOSA-induced apoptosis and examined the lysosomal metabolic perturbations that may underlie the observed cytotoxicity.

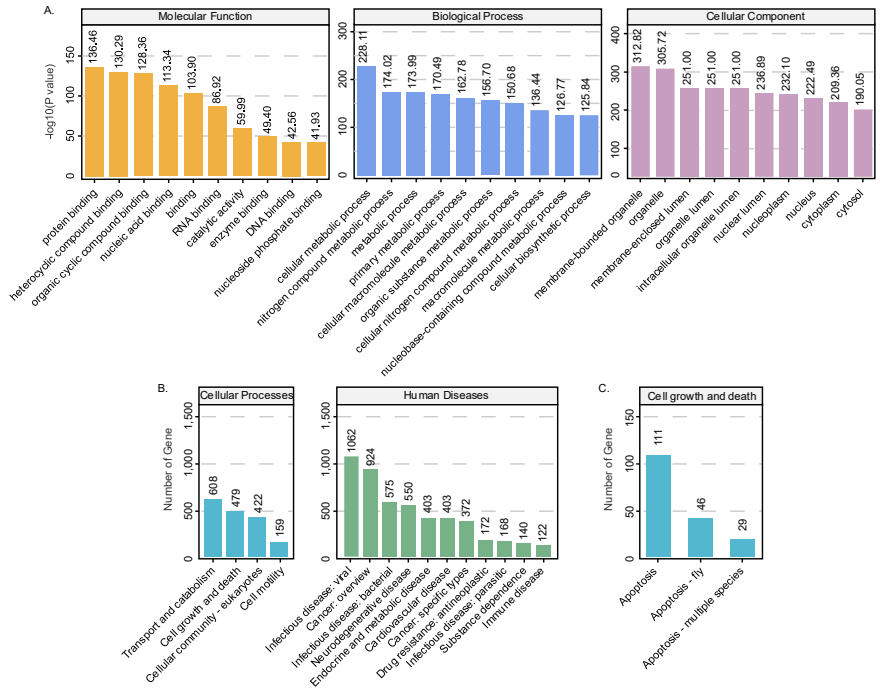



**Fig. 4.** Transcriptomic signature of HK2 cells exposed to 5 μM PFOSA for 3.5 d. (A) Gene Ontology enrichment: differentially expressed genes ($|\log_2 FC| \geq 1.5$, FDR < 0.001) were significantly enriched for "protein binding," "catalytic activity," and "nucleus" among molecular-function, biological-process, and cellular-component terms. (B) KEGG pathway analysis: "cell growth and death," "apoptosis," "endocrine and metabolic diseases," and "infectious disease" pathways were markedly activated. (C) Overview of the "cell growth and death" pathway module.

### 3.5. PFOSA exposure disrupts lysosomal metabolism via GLA suppression

The RNA-seq dataset was intersected with "acute kidney injury" gene sets curated in GeneCards, ClinVar, and the Comparative Toxicogenomics Database (CTD). This cross-database comparison yielded one core hit, the fusion transcript RPL36A-HNRNPH2 (Fig. 5A). The RPL36A-HNRNPH2 fusion transcript was markedly up-regulated in the volcano plot of differentially expressed transcripts (Fig. 5B; $\log_2 FC = 1.560$, $P = 0.0005$), suggesting that this chimeric transcript may act as a key driver of PFOSA-evoked tubular toxicity.

Genomic coordinate inspection revealed that GLA (Xq22.1) is physically bracketed by RPL36A (Xq22.1) and HNRNPH2 (Xq22.1), with all three genes arranged head-to-tail within the same topologically associating domain (Fig. 5C). Consistent with this, RNA-seq data showed that PFOSA-induced up-regulation of the RPL36A-HNRNPH2 fusion transcript was accompanied by a significant decrease in GLA expression (Fig. 5D). This pattern is consistent with transcriptional read-through from RPL36A into HNRNPH2, which relegates the intervening GLA locus to an "intron-like" status, thereby silencing its transcription. GLA encodes lysosomal α-galactosidase A, which hydrolyses globotriaosylceramide (Gb3) to lactosylceramide, thereby sustaining normal lysosomal catabolism. Reduced GLA expression would therefore be expected to provoke intralysosomal Gb3 accumulation. Indeed, ELISA and western blot quantification of cell lysates after 3.5-day exposure to 5 μM PFOSA revealed a significant decline in GLA protein levels in HK2 cells (Fig. 5E), accompanied by a concomitant

increase in Gb3 content (Fig. 5F). Cell lysates were subsequently collected from PFOSA-treated HK2 cells overexpressing GLA, and western blot quantification showed that GLA protein levels were significantly up-regulated (Fig. 5G), with a concomitant decrease in Gb3 content (Fig. 5H).

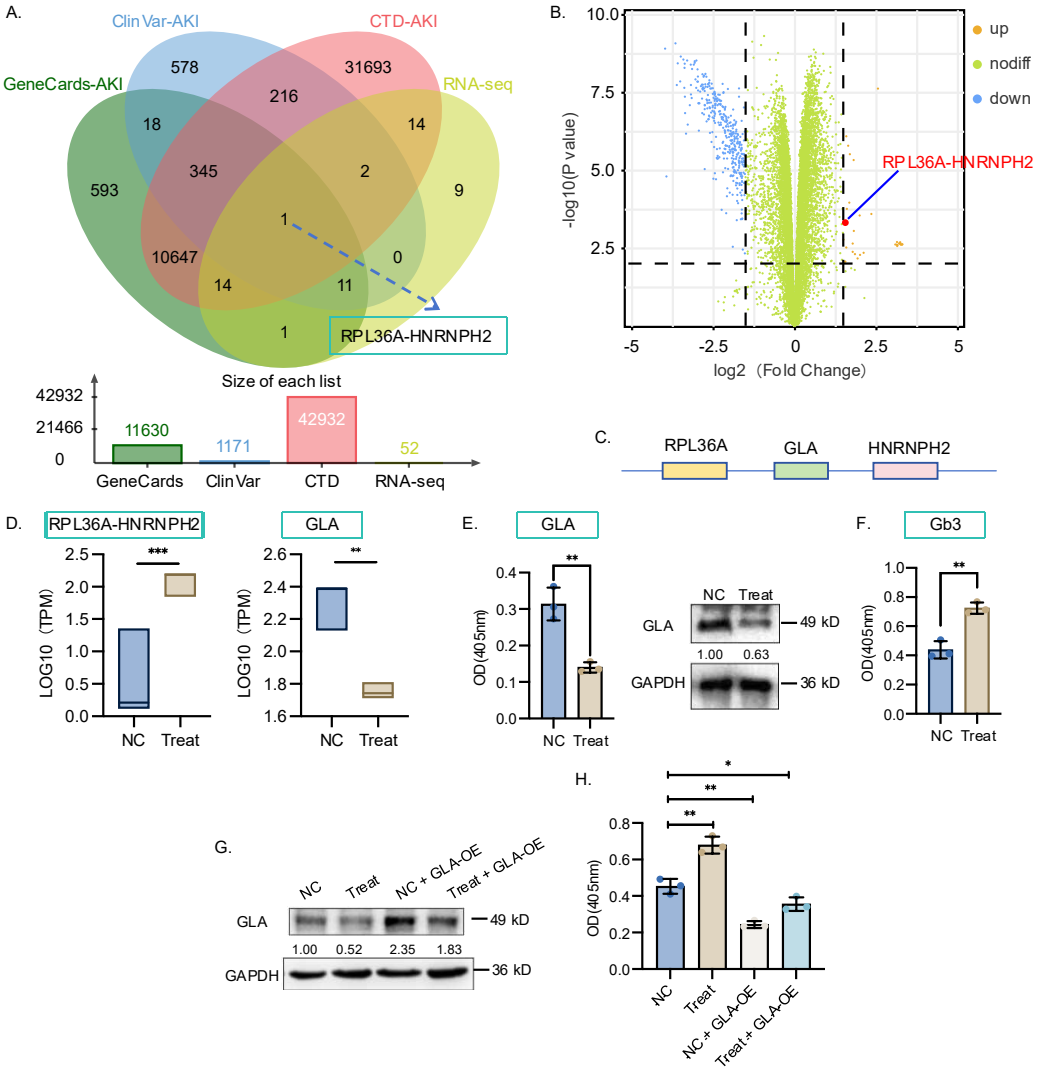



**Fig. 5.** Multi-database intersection and experimental validation identify a core susceptibility gene for PFOSA-induced AKI. (A) Venn diagram: intersection of "acute kidney injury" gene sets from GeneCards, ClinVar, and CTD with RNA-seq DEGs ($|\log_2 FC| \geq 1.5$, FDR < 0.001) yielded one overlapping gene. (B) Volcano plot: the RPL36A-HNRNPH2 fusion transcript (red) resides in the most significantly up-regulated region. (C) Gene architecture: GLA is interposed between RPL36A and HNRNPH2. (D) RNA-seq quantification: PFOSA exposure significantly increased RPL36A-HNRNPH2 and decreased GLA expression in HK2 cells. (E) Quantification of GLA by ELISA and western blot. GLA protein levels declined in HK2 cells after PFOSA exposure. (F) ELISA quantification of Gb3. Intracellular Gb3 accumulated in HK2 cells after PFOSA exposure, concomitant with decreased GLA protein. (G) Western blot quantification of GLA in HK2 cells following PFOSA treatment and GLA overexpression. (H) ELISA quantification of Gb3. Intracellular Gb3 levels significantly decreased in HK2 cells after PFOSA treatment and GLA overexpression. Data are mean ± SD; $^{*}P < 0.05$, $^{**}P < 0.01$, $^{***}P < 0.001$, $^{****}P < 0.0001$; n = 3

### 3.6. PFOSA exposure promotes apoptosis and AKI via NF-κB pathway activation.

Transcriptomic profiling revealed that the core AKI signature genes KIM-1, DKK3, IL18, NAGLU, TIMP2, and IGFBP7 were significantly up-regulated under PFOSA exposure (Fig. 6D、E). However, OPN showed no significant change, which closely mirrors the qPCR data presented in Fig. 2. These results support the conclusion that exposure to sub-cytotoxic levels of PFOSA is sufficient to induce a canonical AKI transcriptional signature in renal tubular epithelial cells.

RNA-seq analysis of the NF-κB signaling pathway revealed that PFOSA exposure simultaneously activated pro-apoptotic signaling and inhibited anti-apoptotic mechanisms. The expression of NF-κB, p50, and p52 was significantly increased (Fig. 6A), whereas the expression of anti-apoptotic factors BIRC2 and BIRC5 was markedly decreased. Notably, the pro-apoptotic effectors FAS and HRK were also down-regulated, while TP53 was strongly up-regulated (Fig. 6C). This paradoxical transcriptional pattern suggests that PFOSA reprograms NF-κB signaling, shifting the balance toward TP53-driven apoptosis independently of classical FAS/HRK-mediated death receptor pathways. Western blot analysis further confirmed that PFOSA exposure decreased total IκBα and increased phosphorylated IκBα (p-IκBα), indicative of canonical NF-κB pathway activation (Fig. 6B). This dual transcriptional program suggests that PFOSA increases tubular epithelial apoptosis by enhancing NF-κB nuclear translocation while suppressing its canonical cytoprotective targets and enforcing a TP53-dependent death program.

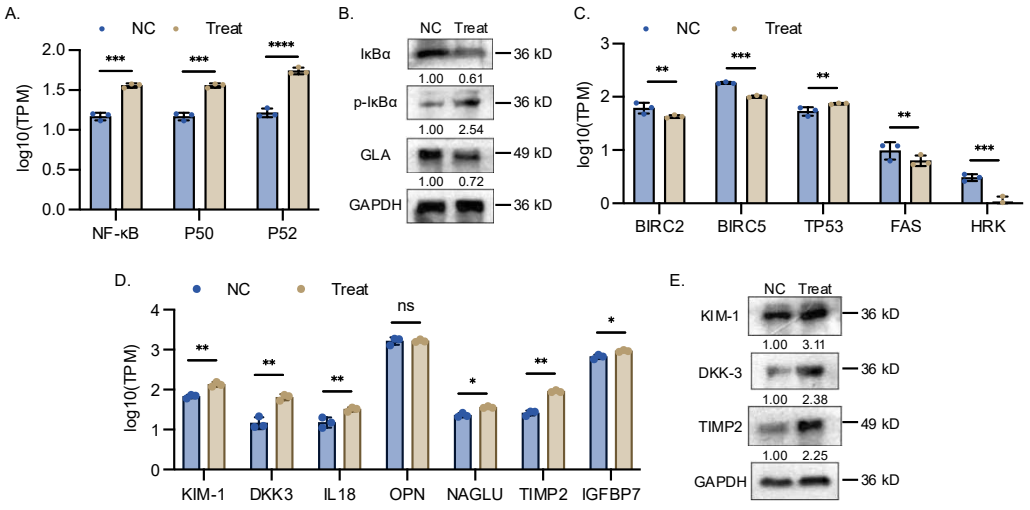



**Fig. 6.** Transcriptomic evidence that PFOSA triggers apoptosis and AKI via NF-κB pathway activation. (A) Expression of NF-κB and its core subunits p50 and p52 was significantly elevated after PFOSA exposure. (B) Western blot analysis. GLA and IκBα protein levels decreased, whereas phosphorylated IκBα (p-IκBα) increased after PFOSA exposure. (C) Within the NF-κB signaling axis, anti-apoptotic genes BIRC2 and BIRC5 were markedly down-regulated, whereas pro-apoptotic TP53 was up-regulated; notably, FAS and HRK were also decreased, suggesting a non-canonical pro-apoptotic reprogramming. (D) mRNA levels of KIM-1, DKK3, IL-18, NAGLU, TIMP2, and IGFBP7 were all significantly increased, consistent with the RT-qPCR trends shown in Fig. 2. (E) Western blot analysis. The AKI signature proteins KIM-1, DKK3, and TIMP2 were up-regulated following PFOSA exposure. Data are mean ± SD; *$P < 0.05$, **$P < 0.01$, ***$P < 0.001$, ****$P < 0.0001$; n = 3.

## 4. Discussion

An increasing body of monitoring data reveals that PFOS has become one of the most persistent emerging organic contaminants on a global scale. It is detected with near-100% frequency from polar snowpacks to urban aquifers, spanning six orders of magnitude in concentration. In China's major river basins, the mean levels of PFOS and PFOA in surface water are 8.7 ng/L and 5.2 ng/L, respectively; however, industrial seepage pits can reach concentrations of up to 38 μg/L—more than 4,000 times higher[13,14]. Even more alarmingly, PFAS have half-lives of 3–5 years and biomagnify at every level of the food chain. Fish, eggs, and breast milk often contain microgram-per-kilogram concentrations, creating a continuous exposure cycle among the environment, diet, and humans[15-17].

Pooled serum analyses show that the global median for PFOS in the general population is around 15 ng/mL, whereas workers in high-exposure occupations can exceed 1 μg/mL—nearly a 70-fold increase [18-21]. These internal doses mirror epidemiological findings in a clear dose–response manner: the higher the serum burden, the greater the increase in immunosuppression, declining thyroid hormones, gestational hypertension, and elevated cholesterol[15]. A mechanistic study of rat renal tubular epithelial cells showed that PFOS increased Sirt1 expression. The excess deacetylase then silenced PPARγ by removing its acetyl tags, forcing the receptor to release its co-activator PGC-1α. Without the PPARγ–PGC-1α complex, transcription of the antioxidant triad (GPx, CAT, and SOD) plummets, pushing the redox balance toward oxidation. At the same time, Sirt1 deacetylates p53, increasing its affinity for Bax. The TP53–Bax complex then translocates to the mitochondria, where it perforates the outer membrane and releases cytochrome c into the cytosol. This activates caspase-3, sealing the tubular cell's fate: apoptosis[22]. Our data showed that HK2 proximal tubular epithelial cells displayed early apoptotic signatures and AKI biomarkers at 5 μM (roughly 2.5 μg/mL)—a level that sits within the reported serum range for occupationally exposed adults; comparable apoptotic trends were also observed in 293T embryonic kidney cells, although these cells are not authentic renal tubular epithelia and were included only to assess the cell-type generality of the pro-apoptotic response. Notably, 5 μM approaches the 4-day IC50 (4.937 μM) determined in this study, indicating that these phenotypes manifest at the threshold between sub-lethal stress and overt cytotoxicity. Future dose–response studies using lower, clearly sub-cytotoxic concentrations (e.g., 1–2 μM) will be essential to confirm that AKI biomarker elevation and early apoptosis occur independently of generalized cell death. Mechanistically, this aligns the "environmentally relevant concentration" hypothesis with tangible tubular injury in vitro. Supporting this, a recent analysis of a neonatal cohort found that a 10 ng/mL increase in maternal serum PFOS reduces offspring glomerular filtration rate by 2.3 mL/min; the underlying renal lesion remains to be elucidated[23]. The dual mechanism identified in our transcriptomic and phenotypic analyses—NF-κB–driven pro-apoptotic signaling coupled to putative GLA silencing and lysosomal Gb3 accumulation—may represent a missing molecular link through which PFAS reprogram renal tubular cell fate. Nevertheless, because the causal chain from PFOSA exposure to NF-κB reprogramming and from the putative RPL36A–HNRNPH2 fusion to GLA silencing remains

correlative, functional rescue experiments (e.g., BIRC2/5 overexpression, NF-κB pharmacological inhibition, or CRISPR-based modulation of the fusion locus) are warranted to establish definitive causality(Fig. 7).

Conventional wisdom portrays NF-κB as the tubular epithelium's "guardian of survival," activating anti-apoptotic genes such as BIRC2/5, CFLAR, and XIAP to stabilize mitochondrial membrane potential and control caspase-3[24-26]. Here, our transcriptomic data reveal that when renal tubular epithelial cells (HK2) encounter PFOSA at concentrations near the 4-day IC50 (5 μM for 3.5 days), the p50/p52 DNA-binding subunits of NF-κB are strongly induced. However, the canonical cytoprotective program collapses: transcripts of BIRC2/5, FAS, and HRK plummet, while the pro-apoptotic TP53 gene surges. In other words, the pollutant appears to reprogram NF-κB, potentially transforming it from a survival switch into a death accelerator[27,28].

This paradox is not without precedent. In cadmium-driven nephrotoxicity, concurrent IKKβ–p65 activation and H3K9me2 deposition at the BIRC3 promoter silence the gene, demonstrating that "epigenetic reprogramming" can strip NF-κB of its cytoprotective arsenal and convert the pathway into a pro-death force[29]. We hypothesize that elevated ROS—consistent with prior reports that PFOSA boosts intracellular H2O2 at comparable concentrations (Jose et al., 2024)—may cause p50 homodimers to bind to the κB motifs within the p53 promoter, transactivating TP53 while oxidative lesions cripple the transcription of anti-apoptotic genes, tipping the balance irreversibly toward cell death[30]. Notably, at its $IC_{50}$ concentration PFOSA already boosts intracellular $H_2O_2$ by 2.8-fold—enough oxidative fuel to switch NF-κB from guardian to executioner[31]. Thus, the ROS–p50–TP53 axis appears to be the master switch that flips NF-κB toward apoptosis. Structural studies demonstrate that p50 homodimers lack a transactivation domain (TAD) and must partner with p65 or Bcl-3 to stimulate cytoprotective transcription. When PFOS suppresses TAK1 and blocks p65 phosphorylation, p50/p50 is left in a transcriptionally inert state and instead recruits HDAC1/DNMT3a, compacting chromatin and extinguishing anti-apoptotic gene expression[32-34].

Our RNA-seq data revealed a significant increase in DNMT3a expression, providing transcriptomic support—though not functional proof—for the "repressive homodimer" hypothesis. A parallel phenotype—NF-κB nuclear translocation coupled with BIRC downregulation—has been observed in a PFOSA testicular model, in which ectopic BIRC2 overexpression rescued 60% of apoptosis. This underscored the critical role of the BIRC family in PFAS-triggered cell death[35-38]. In summary, perfluorooctane derivatives may hijack the NF-κB network in renal epithelia via a proposed three-step process: ROS ignition, epigenetic rewriting, and enforced p50 homodimer recruitment. This model suggests a shift from survival to apoptosis—an unconventional mode that challenges the traditional bimodal view of NF-κB signaling. Furthermore, if validated, this mechanism would furnish druggable checkpoints for PFOS nephropathy: restoring BIRC2/5 levels or disrupting the P50–TP53 interface could offer a novel strategy to prevent renal injury caused by PFAS at environmentally relevant concentrations.

The accumulation of lysosomal globotriaosylceramide (Gb3) has long been considered the molecular

hallmark of Fabry disease. In the canonical cascade, mutations in the GLA gene abolish the activity of the enzyme α-galactosidase A, allowing Gb3 to accumulate inside the endothelium of renal, cardiac, and vascular tissues. The engorged lysosomes eventually rupture, releasing cathepsins and igniting the mitochondrial death pathway, which culminates in apoptosis and multi-organ fibrosis[39-42]. Our study is the first to apply this monogenic metabolic signature to the field of environmental toxicology. RNA-seq analysis identified a putative RPL36A–HNRNPH2 read-through fusion transcript spanning the Xq22.1 topologically associating domain. If this chimeric transcript is confirmed by targeted RT-PCR and Sanger sequencing, it could potentially silence GLA by relegating the intervening locus to an "intron-like" status, thereby reducing enzyme levels and leaving its substrate, Gb3, to accumulate and cause lysosomal swelling. This intriguing overlap between an environmental insult and an inborn error is reminiscent of prior findings that benzo[a]pyrene can evoke Gilbert's syndrome by lncRNA read-through silencing of UGT1A1, underscoring that pollutants can mimic Mendelian disease at the molecular level[43]. At the population level, classical Fabry disease affects approximately one in 40,000 hemizygous males. However, heterozygous females can also accumulate Gb3 to varying degrees due to skewed X-inactivation and develop late-onset renal injury[44-46].

We therefore hypothesize that these "sub-clinical" GLA carriers are uniquely vulnerable; chronic, low-level PFAS exposure could cause them to reach the Gb3 toxicity threshold earlier than the general population. Mechanistically, the accumulating Gb3 amplifies apoptosis through two converging routes: (i) lysosomal membranes rich in cholesterol/Gb3 microdomains expand, recruiting and activating cathepsin B, which initiates the mitochondrial caspase-3 cascade; (ii) Gb3 docks to VDAC2, locking the mitochondrial permeability transition pore (mPTP) in an open state. This results in the collapse of ATP synthesis and the creation of a positive feedback loop with the well-documented mitochondrial toxicity of PFOS[15,47,48]. Notably, while our transcriptomic data are consistent with this lysosome–mitochondria crosstalk model, direct experimental evidence for cathepsin B activation or mPTP opening in PFOSA-exposed renal cells remains to be obtained. In summary, PFOSA may represent the first documented link between an environmental pollutant and a Fabry-like metabolic disorder through a putative RPL36A–HNRNPH2 read-through fusion that appears to transcriptionally silence GLA, pending independent experimental validation. This paradigm offers a new perspective on understanding inter-individual vulnerability to PFOS. Prospective birth cohorts integrating GLA-carrier screening with single-cell multi-omics are now needed to test whether the "low GLA + high PFOSA" signature constitutes an early-AKI risk phenotype, and to determine whether cathepsin B or mPTP inhibitors can halt Gb3-driven tubular apoptosis at real-world exposure levels, opening a precision-intervention avenue against pollutant-triggered nephropathy.

Equally sobering is the fact that conventional potable water treatment, which involves coagulation, sedimentation, and activated carbon, only removes 30% of short-chain PFAS. Switching to reverse osmosis merely shifts the problem, as the retentate still requires disposal, creating a new vector for secondary release. In short, population exposure is unlikely to decrease significantly in the foreseeable future[49-52]. The low-micromolar toxicity

documented here is therefore not merely a curiosity of high-dose laboratory testing, but an accurate reflection of present-day environmental background levels. When deriving health-based guidance values, the exceptional vulnerability of renal tubular epithelium to perfluorooctane derivatives must be considered. We recommend integrating early AKI biomarkers, such as KIM-1 and NAGLU, into routine surveillance and fast-tracking interventions that simultaneously target NF-κB and GLA as twin molecular nodes, thereby curbing the renal health risks posed by ongoing, unavoidable exposure.

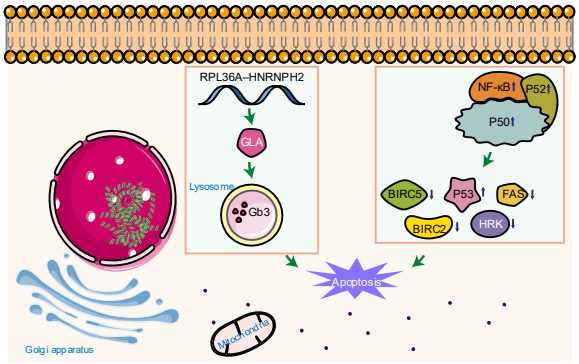



**Fig. 7.** Schematic summarizing the proposed mechanism of PFOSA-induced renal tubular cell apoptosis. PFOSA exposure triggers a putative RPL36A – HNRNPH2 read-through fusion, which transcriptionally suppresses GLA and leads to lysosomal Gb3 accumulation (left). Concurrently, PFOSA activates NF-κB p50/p52 while suppressing anti-apoptotic BIRC2/5, and up-regulates TP53, shifting the balance toward apoptosis (right). The dual perturbation of lysosomal metabolism and NF-κB transcriptional reprogramming converges on tubular epithelial cell death.

## Declarations

### *Ethical Approval and Consent to Participate

This study involved only established human cell lines (HK2 and 293T) and did not involve human subjects or animal experiments; therefore, ethical committee approval was not required.

### *Consent for Publication

All authors have read and approved the final manuscript, agree to be accountable for all aspects of the work, and consent to the submission of this manuscript to the target journal.

### *Data Availability

The data that support the findings of this study are available from the corresponding author upon reasonable request.

### *Funding

This work was supported by the Key Research and Development Program of Yunnan Province (202503AP140034), the National Public Health Talent Cultivation Support Program, and the Yunnan Health Training Project of High Level Talents (L-2024020).

## References

1. Brooke, D., Footitt, A., and Nwaogu, T. (2004). Environmental Risk Evaluation Report: Perflurooctanesulphonate (PFOS).

2. Experts, B.B.G.o. (2021). Guidance on best available techniques and best environmental practices for the use of perfluorooctane sulfonic acid (PFOS), perfluorooctanoic acid (PFOA), and their related substances listed under the Stockholm Convention on Persistent Organic Pollutants.

3. Lee, W.K., Lam, T.K.Y., Tang, H.C., Ho, T.C., Wan, H.T., and Wong, C.K.C. (2023). PFOS-elicited metabolic perturbation in liver and fatty acid metabolites in testis of adult mice. Front Endocrinol (Lausanne) *14*, 1302965. 10.3389/fendo.2023.1302965.

4. Wan, H.T., Zhao, Y.G., Wei, X., Hui, K.Y., Giesy, J.P., and Wong, C.K. (2012). PFOS-induced hepatic steatosis, the mechanistic actions on β-oxidation and lipid transport. Biochim Biophys Acta *1820*, 1092–1101. 10.1016/j.bbagen.2012.03.010.

5. Costello, E., Rock, S., Stratakis, N., Eckel, S.P., Walker, D.I., Valvi, D., Cserbik, D., Jenkins, T., Xanthakos, S.A., Kohli, R., et al. (2022). Exposure to per- and Polyfluoroalkyl Substances and Markers of Liver Injury: A Systematic Review and Meta-Analysis. Environ Health Perspect *130*, 46001. 10.1289/ehp10092.

6. Wan, H.T., Zhao, Y.G., Wong, M.H., Lee, K.F., Yeung, W.S., Giesy, J.P., and Wong, C.K. (2011). Testicular signaling is the potential target of perfluorooctanesulfonate-mediated subfertility in male mice. Biol Reprod *84*, 1016–1023. 10.1095/biolreprod.110.089219.

7. Shi, F., Almerick, T.B.D., Wan, H.T., Chan, T.F., Zhang, E.L., Lai, K.P., and Wong, C.K. (2022). Hepatic metabolism gene expression and gut microbes in offspring, subjected to in-utero PFOS exposure and postnatal diet challenges. Chemosphere *308*, 136196. 10.1016/j.chemosphere.2022.136196.

8. Preisendanz, H., Li, H., Mashtare, M., and Mina, O. (2024). PFAS in agroecosystems: Sources, impacts, and opportunities for mitigating risks to human and ecosystem health. Journal of Environmental Quality *54*, 1–5. 10.1002/jeq2.20670.

9. Stewart, J., Chung, K., Key, P., Wirth, E., and DeLorenzo, M. (2025). Replacement PFAS-free Aqueous Film-Forming foams impact growth more than a PFAS-containing product in the hard clam, Mercenaria mercenaria. Environmental Toxicology and Chemistry. 10.1093/etojnl/vgaf287.

10. Dehghani, M.H., Aghaei, M., Bashardoust, P., Ghalhari, M., Nayeri, D., Malekpoor, M., Sheikhi, S., and Shi, Z. (2025). An insight into the environmental and human health impacts of per- and polyfluoroalkyl substances (PFAS): exploring exposure pathways and their implications. Environmental Sciences Europe *37*. 10.1186/s12302-025-01122-9.

11. Zhang, S., Chen, X., Jin, E., Wang, A., Chen, T., Zhang, X., Zhu, J., Dong, L., Sun, Y., Yu, C., et al. (2025). The GSA Family in 2025: A Broadened Sharing Platform for Multi-Omics and Multimodal Data. Genomics Proteomics Bioinformatics. 10.1093/gpbjnl/qzaf072.

12. Database Resources of the National Genomics Data Center, China National Center for Bioinformation in 2025. (2025). Nucleic Acids Res *53*, D30–d44. 10.1093/nar/gkae978.

13. Li, J.Y., Liu, M.M., and Bi, J. (2025). Characteristics of Spatial and Temporal Distribution of Perfluorinated Compounds (PFCs) in China Surface Water and Health Risk Assessment.

Environmental Monitoring and Forewarning *17*, 1–12.

14. Wang, L.F., Jiang, J., Gong, X.J., Zhou, L., Zhou, H.Y., Zhu, X.X., and Wang, G.Q. (2025). Study on the Spatiotemporal Distribution and Pollution Characteristics of Perfluorinated Compounds in Drinking Water in the Yongzhou Section of the Upper Reaches of the Xiangjiang River. Environmental Monitoring and Forewarning *17*, 137–145.

15. Dourson, M.L., Green, L.C., Crouch, E.A.C., Clewell, H.J., Colnot, T., Cox, T., Dekant, W., Dell, L.D., Deyo, J.A., Gadagbui, B.K., et al. (2025). Estimating safe doses of perfluorooctane sulfonate (PFOS): an international collaboration. Arch Toxicol. 10.1007/s00204-025-04134-9.

16. Podder, A., Sadmani, A., Reinhart, D., Chang, N.B., and Goel, R. (2021). Per and poly-fluoroalkyl substances (PFAS) as a contaminant of emerging concern in surface water: A transboundary review of their occurrences and toxicity effects. J Hazard Mater *419*, 126361. 10.1016/j.jhazmat.2021.126361.

17. Post, G.B. (2021). Recent US State and Federal Drinking Water Guidelines for Per- and Polyfluoroalkyl Substances. Environ Toxicol Chem *40*, 550–563. 10.1002/etc.4863.

18. Li, J., Duan, W., An, Z., Jiang, Z., Li, L., Guo, M., Tan, Z., Zeng, X., Liu, X., Liu, Y., et al. (2024). Legacy and alternative per- and polyfluoroalkyl substances spatiotemporal distribution in China: Human exposure, environmental media, and risk assessment. J Hazard Mater *480*, 135795. 10.1016/j.jhazmat.2024.135795.

19. Pierozan, P., Kosnik, M., and Karlsson, O. (2023). High-content analysis shows synergistic effects of low perfluorooctanoic acid (PFOS) and perfluorooctane sulfonic acid (PFOA) mixture concentrations on human breast epithelial cell carcinogenesis. Environ Int *172*, 107746. 10.1016/j.envint.2023.107746.

20. Suman, T.Y., and Kwak, I.S. (2025). Current understanding of human bioaccumulation patterns and health effects of exposure to perfluorooctane sulfonate (PFOS). J Hazard Mater *487*, 137249. 10.1016/j.jhazmat.2025.137249.

21. Wang, F., Cheng, B., Wu, W., Chen, Y., Dai, J., and Li, Y. (2025). Mechanistic insights into PFOS-induced inflammatory bowel disease: a network toxicology and molecular docking study. Int J Surg *111*, 5150–5161. 10.1097/js9.0000000000002638.

22. Wen, L.L., Lin, C.Y., Chou, H.C., Chang, C.C., Lo, H.Y., and Juan, S.H. (2016). Perfluorooctanesulfonate Mediates Renal Tubular Cell Apoptosis through PPARgamma Inactivation. PLoS One *11*, e0155190. 10.1371/journal.pone.0155190.

23. Lin, P.D., Cardenas, A., Hauser, R., Gold, D.R., Kleinman, K.P., Hivert, M.F., Calafat, A.M., Webster, T.F., Horton, E.S., and Oken, E. (2021). Per- and polyfluoroalkyl substances and kidney function: Follow-up results from the Diabetes Prevention Program trial. Environ Int *148*, 106375. 10.1016/j.envint.2020.106375.

24. Zhang, D., Zhang, Y.H., Liu, B., Yang, H.X., Li, G.T., Zhou, H.L., Wang, Y.S., and Xu, Z.X. (2026). Activation of TLR4-NF-κB signaling in renal tubular epithelial cells facilitates renal allograft fibrosis by inhibiting peroxisome biogenesis. Biochim Biophys Acta Mol Basis Dis *1872*, 168066. 10.1016/j.bbadis.2025.168066.

25. Jiao, Y., and Yang, R. (2025). Berberine alleviates respiratory syncytial virus (RSV)-induced pediatric bronchiolitis and fibrosis via suppressing the HMGB1/TLR4/NF-κB pathway. Microbiol Spectr *13*, e0090025. 10.1128/spectrum.00900-25.

26. Qin, Z.H., Tao, L.Y., and Chen, X. (2007). Dual roles of NF-kappaB in cell survival and implications of NF-kappaB inhibitors in neuroprotective therapy. Acta Pharmacol Sin *28*,

1859–1872. 10.1111/j.1745-7254.2007.00741.x.

27. Lang, Y., Chu, F., Liu, L., Zheng, C., Li, C., Shen, D., Liu, S., Zhang, W., Cui, L., and Zhu, J. (2022). Potential role of BAY11-7082, a NF-κB blocker inhibiting experimental autoimmune encephalomyelitis in C57BL/6J mice via declining NLRP3 inflammasomes. Clin Exp Immunol *207*, 378–386. 10.1093/cei/uxab022.

28. Li, L., Wang, Z., Ma, B., Ye, Q., Lei, Y., Lu, M., Ye, L., Kang, J., Huang, W., Xu, S., et al. (2025). BAY11-7082 Targets RNF25 to Reverse TRIP4 Ubiquitination-dependent NF-κB Activation and Apoptosis Resistance in Renal Cell Carcinoma. Int J Biol Sci *21*, 4410–4427. 10.7150/ijbs.115032.

29. Wang, W., Chen, J., Luo, L., Li, Y., Liu, J., and Zhang, W. (2018). Effect of cadmium on kitl pre-mRNA alternative splicing in murine ovarian granulosa cells and its associated regulation by miRNAs. J Appl Toxicol *38*, 227–239. 10.1002/jat.3516.

30. Shi, T., van Soest, D.M.K., Polderman, P.E., Burgering, B.M.T., and Dansen, T.B. (2021). DNA damage and oxidant stress activate p53 through differential upstream signaling pathways. Free Radic Biol Med *172*, 298–311. 10.1016/j.freeradbiomed.2021.06.013.

31. Jose, E., March-Steinman, W., Wilson, B.A., Shanks, L., Parkinson, C., Alvarado-Cruz, I., Sweasy, J.B., and Paek, A.L. (2024). Temporal coordination of the transcription factor response to H(2)O(2) stress. Nat Commun *15*, 3440. 10.1038/s41467-024-47837-w.

32. Chen, S., Hu, T., Xu, L., Li, J., Liu, C., Zeng, B., Lin, Q., and Cao, Z. (2025). Lactobacillus reuteri SBC5-3 suppresses TNF-α-induced inflammatory responses via NF-κB pathway inhibition in intestinal epithelial cells. Front Microbiol *16*, 1573479. 10.3389/fmicb.2025.1573479.

33. Lu, W., Wang, Y., and Wen, J. (2024). The Roles of RhoA/ROCK/NF-κB Pathway in Microglia

526 Polarization Following Ischemic Stroke. J Neuroimmune Pharmacol *19*, 19.
527 10.1007/s11481-024-10118-w.
528 34. Wei, M., Li, M., Li, Y., Wang, B., Yan, Y., and Li, L. (2025). Upregulation of Receptor Interacting
529 Protein 1 Induced by UVB Contributes to Photodamage of the Skin Through NF-κB Pathway
530 In Vivo and In Vitro. J Cosmet Dermatol *24*, e70082. 10.1111/jocd.70082.
531 35. Teng, Y.N., Chuang, P.J., and Liu, Y.W. (2012). Nuclear factor-κB (NF-κB) regulates the
532 expression of human testis-enriched Leucine-rich repeats and WD repeat domain containing
533 1 (LRWD1) gene. Int J Mol Sci *14*, 625–639. 10.3390/ijms14010625.
534 36. Pentikäinen, V., Suomalainen, L., Erkkilä, K., Martelin, E., Parvinen, M., Pentikäinen, M.O., and
535 Dunkel, L. (2002). Nuclear factor-kappa B activation in human testicular apoptosis. Am J
536 Pathol *160*, 205–218. 10.1016/s0002-9440(10)64364-7.
537 37. Tencer, A.H., Yu, Y., Causse, S.Z., Campbell, G.R., Klein, B.J., Xuan, H., Cartier, J., Miles, M.A.,
538 Gaurav, N., Zadoroznyj, A., et al. (2023). Molecular basis for nuclear accumulation and
539 targeting of the inhibitor of apoptosis BIRC2. Nat Struct Mol Biol *30*, 1265–1274.
540 10.1038/s41594-023-01044-1.
541 38. Yamato, A., Soda, M., Ueno, T., Kojima, S., Sonehara, K., Kawazu, M., Sai, E., Yamashita, Y.,
542 Nagase, T., and Mano, H. (2015). Oncogenic activity of BIRC2 and BIRC3 mutants independent
543 of nuclear factor-κB-activating potential. Cancer Sci *106*, 1137–1142. 10.1111/cas.12726.
544 39. Pande, S., Varzideh, F., Gambardella, J., Jankauskas, S.S., Cerasuolo, F.A., Spinelli, L., Kansakar,
545 U., De Luca, A., Kurland, I.J., Sidoli, S., et al. (2025). Fabry disease cardiomyopathy: A
546 state-of-the-art review. Prog Cardiovasc Dis *92*, 43–65. 10.1016/j.pcad.2025.08.003.
547 40. Živná, M., Dostálová, G., Barešová, V., Mušálková, D., Svojšová, K., Meiseles, D., Kinstlinger, S.,

548 Kuchař, L., Asfaw, B., Poupětová, H., et al. (2025). Misprocessing of α -Galactosidase A,
549 Endoplasmic Reticulum Stress, and the Unfolded Protein Response. J Am Soc Nephrol *36*,
550 628–644. 10.1681/asn.0000000535.
551 41. Al-Obaide, M.A., Al, O., II, and Vasylyeva, T.L. (2022). The potential consequences of
552 bidirectional promoter methylation on GLA and HNRNPH2 expression in Fabry disease
553 phenotypes in a family of patients carrying a GLA deletion variant. Biomed Rep *17*, 71.
554 10.3892/br.2022.1554.
555 42. Al-Obaide, M.A., Islam, S., Al-Obaidi, I., and Vasylyeva, T.L. (2023). Novel enhancer mediates
556 the RPL36A-HNRNPH2 readthrough loci and GLA gene expressions associated with fabry
557 disease. Front Genet *14*, 1229088. 10.3389/fgene.2023.1229088.
558 43. Wang, C.J., Zhang, M.D., Bai, T.Y., Hu, Y.X., Li, J., Wang, L., Su, M., Yang, F., and Chang, F.H.
559 (2023). Benzo[a]pyrene promotes expressions of hepatic gluconeogenesis related molecules
560 through aryl hydrocarbon receptor. Chin J Pharmacol Toxicol *37*, 601–608.
561 44. Tuttolomondo, A., Chimenti, C., Cianci, V., Gallieni, M., Lanzillo, C., La Russa, A., Limongelli, G.,
562 Mignani, R., Olivotto, I., Pieruzzi, F., and Pisani, A. (2025). Females with Fabry disease: an
563 expert opinion on diagnosis, clinical management, current challenges and unmet needs.
564 Front Cardiovasc Med *12*, 1536114. 10.3389/fcvm.2025.1536114.
565 45. Wagenhäuser, L., Rickert, V., Sommer, C., Wanner, C., Nordbeck, P., Rost, S., and Üçeyler, N.
566 (2022). X-chromosomal inactivation patterns in women with Fabry disease. Mol Genet
567 Genomic Med *10*, e2029. 10.1002/mgg3.2029.
568 46. de Alencar, D.O., Netto, C., Ashton-Prolla, P., Giugliani, R., Ribeiro-Dos-Santos, Â., Pereira, F.,
569 Matte, U., Santos, N., and Santos, S. (2014). Fabry disease: Evidence for a regional founder

effect of the GLA gene mutation 30delG in Brazilian patients. Mol Genet Metab Rep *1*, 414–421. 10.1016/j.ymgmr.2014.09.002.

47. Xie, Z., Zhao, M., Yan, C., Kong, W., Lan, F., Narengaowa, Zhao, S., Yang, Q., Bai, Z., Qing, H., and Ni, J. (2023). Cathepsin B in programmed cell death machinery: mechanisms of execution and regulatory pathways. Cell Death Dis *14*, 255. 10.1038/s41419-023-05786-0.

48. Pieroni, M., Ciabatti, M., Graziani, F., Camporeale, A., Saletti, E., Lillo, R., Figliozzi, S., and Bolognese, L. (2022). The Heart in Fabry Disease: Mechanisms Beyond Storage and Forthcoming Therapies. Rev Cardiovasc Med *23*, 196. 10.31083/j.rcm2306196.

49. Zhang, M.M., Tian, Q., An, Z.Y., and Xu, C.X. (2025). Research Progress on the Sources, Analysis Methods and OccurrenceCharacteristics of Per- and Polyfluoroalkyl Substances in the Environment. Research of Environmental Science *38*, 677–687. 10.13198/j.issn.1001-6929.2025.01.04.

50. Chen, Y., Zhang, H., Liu, Y., Bowden, J.A., Townsend, T.G., and Solo-Gabriele, H.M. (2024). Evaluation of per- and polyfluoroalkyl substances (PFAS) released from two Florida landfills based on mass balance analyses. Waste Manag *175*, 348–359. 10.1016/j.wasman.2023.12.054.

51. Liu, Y., Robey, N.M., Bowden, J.A., Tolaymat, T.M., Solo-Gabriele, H.M., and Townsend, T.G. (2025). A Componential Evaluation of Per- and Polyfluoroalkyl Substances (PFAS) in Municipal Solid Waste (MSW) Streams. Environ Sci Technol. 10.1021/acs.est.5c16358.

52. Quinete, N., Tansel, B., Katsenovich, Y., Ocheje, J.O., Mendoza Manzano, M., and Nasir, Z. (2025). Leaching profile of per- and polyfluoroalkyl substances from selected e-waste components and potential exposure pathways from discarded components. J Hazard Mater

592 *491*, 137953. 10.1016/j.jhazmat.2025.137953.

593

## Supplementary Files

This is a list of supplementary files associated with this preprint. Click to download.

- SupplementaryTable1.xlsx
- Supplementarydata.docx
- Scan0001.pdf